Chapter 4

VISIBLE TWO-DIMENSIONAL PHOTONIC CRYSTAL SLAB LASERS

4.1 Introduction

Photonic crystal cavities offer many advantages over more conventional cavities for achieving ultra-small modal volumes while maintaining high quality factors [1-5]. When combining such cavities with light emitting active materials, such as quantum wells (QWs) [1] and quantum dots (QDs) [3], it is possible to form ultra-small lasers that can be integrated in dense arrays, and in which each laser cavity supports only very few optical modes. This results in the potential for high frequency modulation of such lasers [6], which has made these devices particularly interesting for applications in optical data communication. Therefore, most research on photonic crystal lasers has thus far focused on near-infrared wavelength emission using InGaAsP or InGaAs active materials. Although some research groups have started to explore the visible wavelength range [7-10], it has been difficult to obtain small mode volume lasers in visible light emitting material systems due to high surface carrier recombination velocities or the lack of high refractive index contrast substrates for light confinement in the vertical direction. Visible photonic crystal lasers operating in the spectral vicinity of 670 nm could enable a broad range of important applications, including high-density optical recording, high resolution visible laser projection displays, and, most importantly, compact spectroscopic sources as ultra-small sensors for biological and chemical detection within small sample volumes. The same devices, when operated in reverse bias, can also function as multispectral detector arrays,

which can be used for polarization-sensitive detection in the visible and near-IR wavelength range. In this chapter, we present our preliminary experimental results of such a two-dimensional photonic crystal slab laser that can satisfy these needs.

4.2 Two-dimensional photonic crystal slab structure

Photonic crystal slab structures were first grown by metallorganic chemical vapor deposition (MOCVD) of InGaP/InGaAlP quantum well material on top of sacrificial AlGaAs layers supported by GaAs substrates. Optical gain was provided by two 7 nm thick and compressively strained InGaP quantum wells which were separated by 10 nm InGaAlP

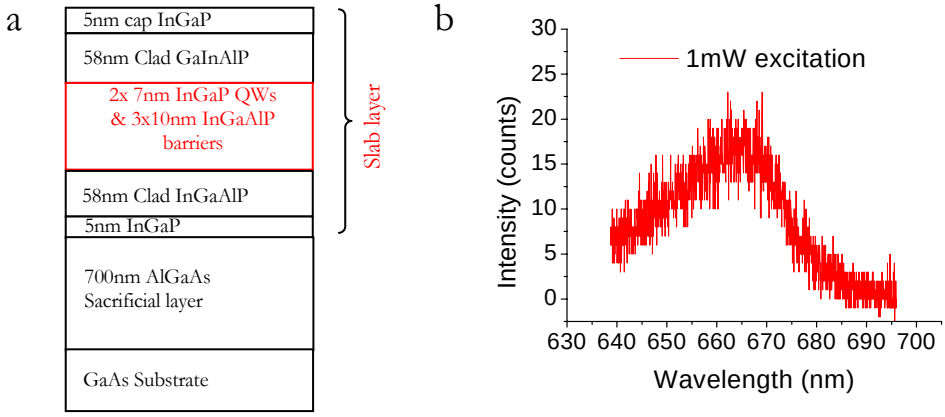

Figure 4.1. Scanning electron microscope image of photonic crystal laser cavity: (a) low-magnification image showing the entire device and (b) higher-resolution image showing the details of the cavity

barriers (Figure 4.1a). The quantum well active material was placed in the center of a 170 nm thick InGaAlP slab, with a 700 nm thick sacrificial AlGaAs layer between the slab and the GaAs substrate. The active quaternary material was designed to emit light at around 670 nm (Figure 4.1b). From the compressive strained quantum wells, light was strongly

coupled into transverse electric (TE) modes. This epitaxially grown material was coated with a 100 nm SiON hard mask and 200 nm of ZEP520 electron beam resist.

Electron beam lithography was then used to define the photonic crystal cavity pattern within the ZEP520 resist. Reactive ion etching (RIE) was subsequently used to transfer the pattern from that resist into the SiON etch mask by using a CHF_3 plasma. After removal of the resist, the hard mask pattern was further transferred through the active layer with an iodine-based inductively coupled plasma reactive ion etch (ICP-RIE). Time-controlled oxidation of the AlGaAs by water vapor followed by the potassium hydroxide (KOH) chemical dissolution of the aluminum oxide formed the suspended slab membranes as shown in Figure 4.2. Finally, diluted buffered hydrofluoric acid was used to remove the SiON etch mask.

The suspended photonic crystal slab cavities were optically pumped at room temperature using 5 ns pulses at 10 kHz (0.005% duty cycle) with a 408 nm InGaN semiconductor diode laser. The pump beam was focused onto the sample surface with a 50x objective lens to form an excitation beam spot size about 2 μm in diameter. The excitation power used in this chapter was determined by dividing the averaged pulse power by the duty cycle. The emission from the lasers was then collected through the same lens and their spectra detected with a liquid-nitrogen-cooled charge-coupled device (CCD) (Princeton instruments, Spec10) detector filtered by a monochromator (Acton, SpectraPro). The monochromator entrance slit width was set to 10μm and the 1200 g/mm grating was used, resulting in a spectral resolution of approximately 0.1 nm. An additional flip-up

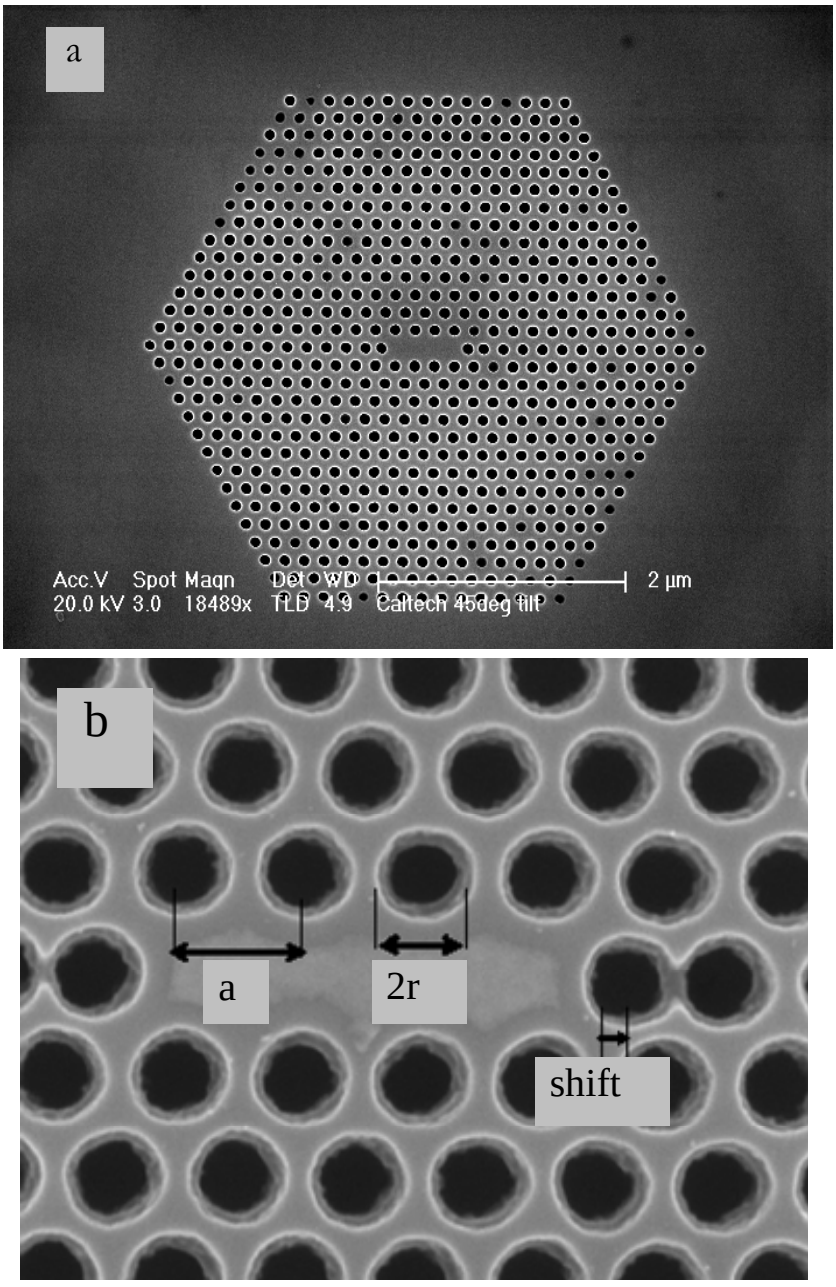

Figure 4.2. Scanning electron microscope image of photonic crystal laser cavity (a) low magnification image showing the entire device and (b) higher resolution image showing the details of the cavity.

mirror was used to guide the light into a CCD imaging system to view the near-field images of the lasers as well as the excitation laser spot. The imaging optics also permitted the observation of laser cavity modes.

4.3 Characterization of the 2D photonic crystal slab laser

For this work, we used a high Q cavity design proposed by Noda's group [5] consisting of a L3 linear defect (removing 3 holes) within a triangular photonic crystal lattice of holes on a thin high-index slab. This design reduces the loss in the vertical direction by shifting the holes at the end of the defect area outwards. Figure 4.2 shows the top view of a fabricated photonic crystal microcavitiy slab. The lattice spacing, a, the radius of hole, r, and the shift of the hole were defined as shown in the Figure 4.2b. We lithographically controlled the ratio between the hole shift and the lattice spacing (shift/a) to be 0.2. Also, we lithographically varied the lattice spacing (a) within a range from 0.14 μm to 0.18 μm and the ratio between the hole radius and lattice spacing (r/a, the porosity factor) from 0.25 to 0.29. Fourteen periods of photonic crystal lattice (Figure 4.2a) were used to surround the defect within the 170 nm thick quantum well active layer slab, which has a refractive index of around 3.4 at 670 nm. The photonic crystal and cavity dimensions were designed to match the 670 nm emission wavelength of the InGaP active material. Figure 4.3 shows luminescence spectra and the L(excitation power)-L(lasing peak intensity) curve from a device with lattice parameter a=170 nm and porosity factor r/a=0.26. The laser threshold was determined to be approximately 250 μW, and the linewidth was measured as 0.3 nm at threshold, yielding an effective Q of about 2000. Below threshold, only a broad background from the gain medium was measured from this cavity. Above 450 μW, heating of the laser cavity limited the output power, and the L-L curve saturated. The 2D photonic crystal cavity peak can be tuned by changing either the porosity or the lattice parameter of the photonic crystal lattice surrounding the nanocavity. Figure 4.4 shows a laser with a slightly lower porosity (porosity factor r/a=0.25). For this laser, the measured

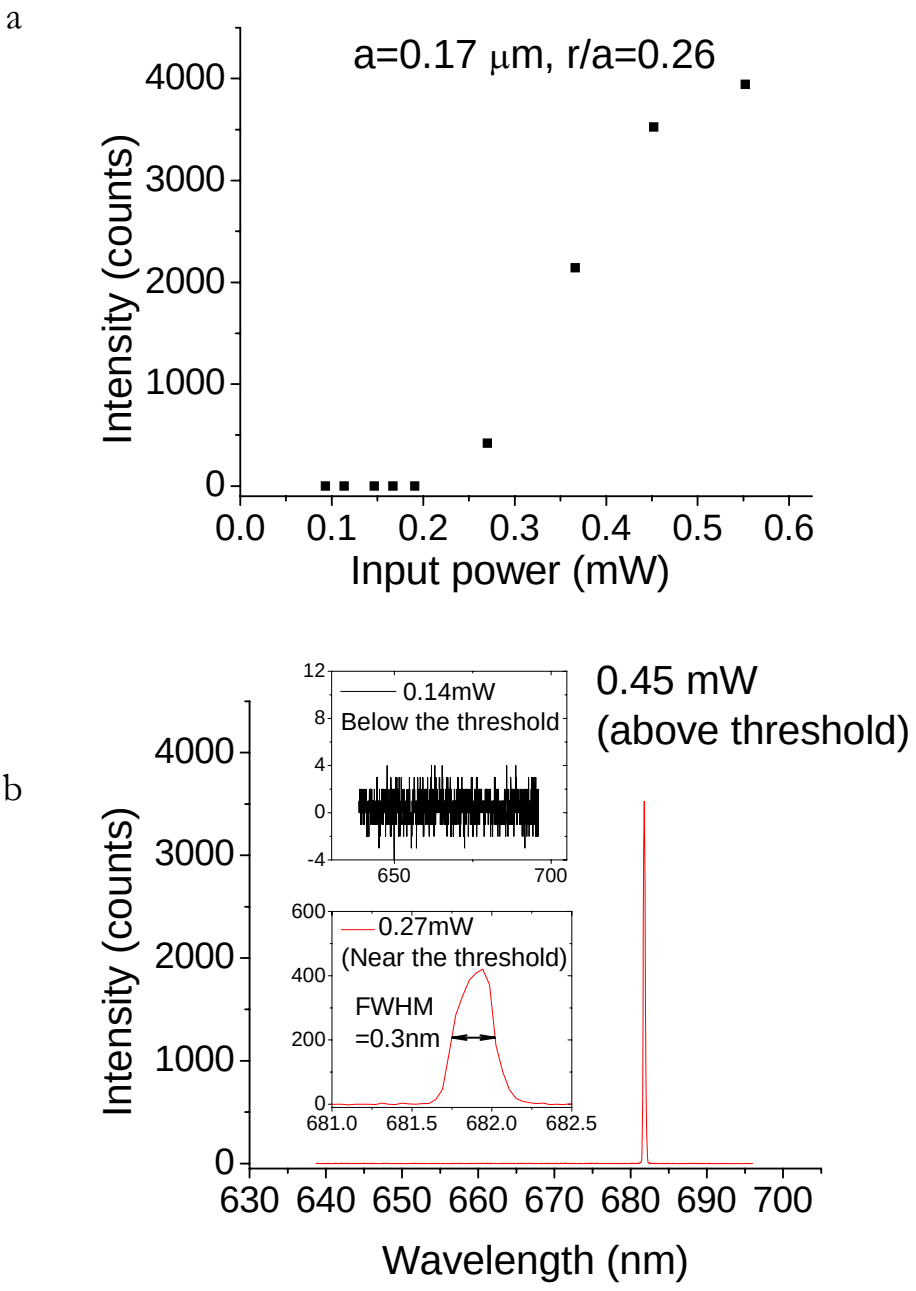

Figure 4.3. (a) L-L curve. (b) Typical lasing spectrum of an InGaP 2D photonic crystal laser with a lattice parameter of a=0.17 μm and porosity factor r/a=0.26

laser threshold was 400 μW, and the device again saturated as a result of cavity heating above 1 mW. Both cavities exhibited distinct threshold and linearity in the output power

a

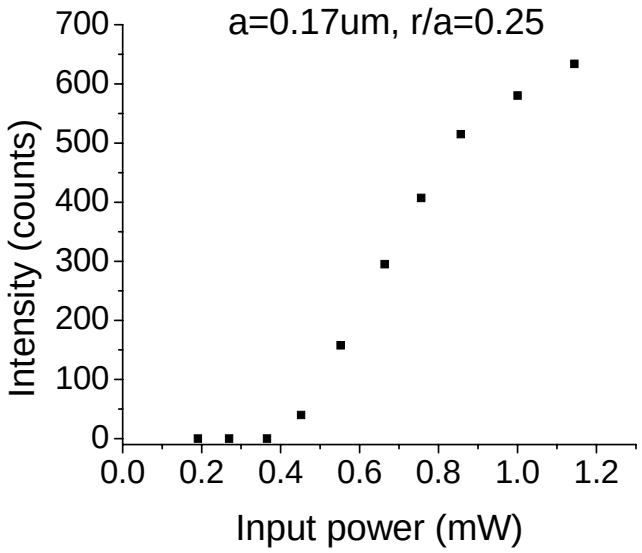

b

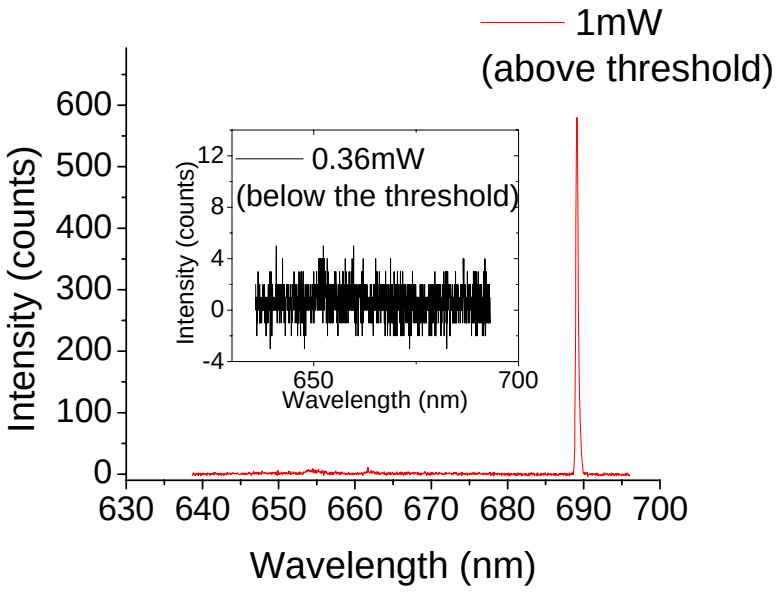

Figure 4.4. (a) L-L curve. (b)Typical lasing spectrum for an InGaP 2D photonic crystal laser with a lattrice parameter of a=0.17 μm and a porosity factor r/a=0.25

above threshold but before saturation. The lasing characteristic was very sensitive to the position of the excitation beam spot (~1 μm movement), which indicates that lasing occurs from a localized defect mode. Many of the photonic crystal cavity geometries that we defined did not result in demonstration of lasing, and we show a typical spectrum result

from a non-lasing cavity in Figure 4.5, along with the L-L curve. In this case, no inflection was measured and a more or less linear increase of emission with increasing excitation power was observed, saturating again at high excitation powers due to heating of the cavity. No lasing peak was observed, and the Fabry-Perot filtered luminescence emission was not bright enough to observe with our experimental spectroscopic measurement setup.

4.4 Tuning of the emission peak wavelength

Figure 4.6a shows the influence of changing of the porosity on the laser emission wavelength, whereas Figure 4.6b shows a similar tuning curve for changes in the photonic crystal lattice parameter. The uneven spectral shifts result from fabrication variation and device scaling only in two rather than three dimensions due to the fixed slab thickness. This data indicates that the InGaP photonic crystal lasers can be lithographically tuned throughout the gain emission of the quantum wells. The accuracy of such tuning is only limited by the quality and reproducibility of the fabrication process. It should be noted that the minimum feature size required for the successful definition of the photonic crystal mirror surrounding the laser cavities is approximately 30 nm, which is the distance between two adjacent holes in the slab. Compared to conventional InGaAsP material systems operating at 1550 nm, our fabrication process has to overcome the feature size scaling associated with the 2.3 times decreases in wavelength. Nevertheless, with our fabrication approach, it is possible to define dense arrays of laser cavities that are separated by as little as 2 microns. Compact multi-spectral sources can therefore be defined within the visible wavelength range.

a

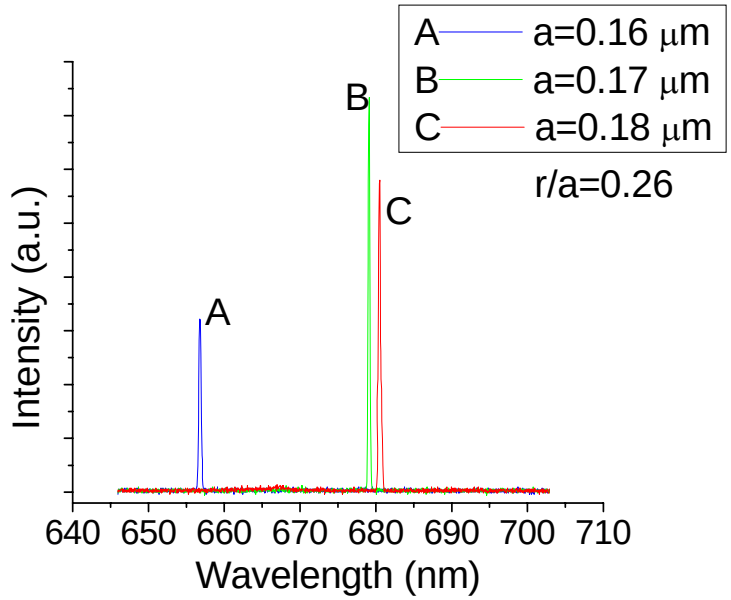

b

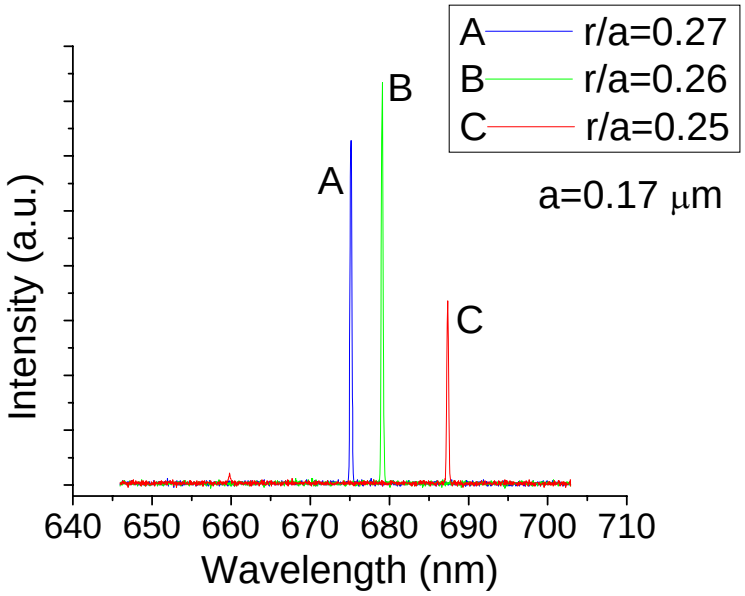

Figure 4.5. (a) r/a fixed to 0.26. (b) Lattice spacing fixed to 0.17 μm (the uneven spectral shifts result from fabrication variation and device scaling only in two dimensions due to the fixed slab thickness)

4.5 Conclusion

The use of photonic crystal lasers for spectroscopic analysis has been described earlier [11], and offers the opportunity to define ultra-small optical cavities with enormous optical field intensities. These devices have been used in the past as refractive index sensors, indicating the refractive index of volumes as small as 10^{-17} liters, limited by the mode volume of 0.03 cubic microns at 1550 nm wavelength. In our experiments, we have defined lasers within a wavelength range that is even more interesting for spectroscopic applications, as many of the fluorophores used for biological analysis are limited to the visible spectrum, and single-photon detectors are available at such wavelengths. Moreover, these devices may become very interesting sources for Raman spectroscopy and other specific measurements of the chemical composition of the femtoliter contents of an optical nanocavity. We expect InGaP lasers to be very useful for biochemical analysis as well as for efficient displays and high-frequency lasers in the near future.

Bibliography

1. Painter, O., et al., *Two-dimensional photonic band-gap defect mode laser.* Science, 1999. **284**(5421): 1819-1821.
2. Loncar, M., et al., *Low-threshold photonic crystal laser.* Applied Physics Letters, 2002. **81**(15): 2680-2682.
3. Yoshie, T., et al., *Quantum dot photonic crystal lasers.* Electronics Letters, 2002. **38**(17): 967-968.
4. Vahala, K.J., *Optical microcavities.* Nature, 2003. **424**(6950): 839-846.
5. Akahane, Y., et al., *High-Q photonic nanocavity in a two-dimensional photonic crystal.* Nature, 2003. **425**(6961): 944-947.

6. Yoshie, T., et al., *High frequency oscillation in photonic crystal nanolasers.* Applied Physics Letters, 2004. **84**(18): 3543-3545.

7. Campbell, M., et al., *Fabrication of photonic crystals for the visible spectrum by holographic lithography.* Nature, 2000. **404**(6773): 53-56.

8. Wu, X., et al., *Ultraviolet photonic crystal laser.* Applied Physics Letters, 2004. **85**(17): 3657-3659.

9. Choi, Y.S., et al., *GaN blue photonic crystal membrane nanocavities.* Applied Physics Letters, 2005. **87**(24)

10. Meier, C., et al., *Visible resonant modes in GaN-based photonic crystal membrane cavities.* Applied Physics Letters, 2006. **88**(3)

11. Loncar, M., A. Scherer, and Y.M. Qiu, *Photonic crystal laser sources for chemical detection.* Applied Physics Letters, 2003. **82**(26): 4648-4650